Proceedings of the International Symposium on Near-Earth Objects
United Nations/Explorers Club, New York, April 24-26, 1995.

Comet Shoemaker-Levy 9 Fragment Size Estimates: How big was the Parent Body?

David A. Crawford

Computational Physics and Mechanics Department 9232
P. O. Box 5800, MS 0820
Sandia National Laboratories
Albuquerque, NM 87185-0820

Abstract

The impact of Comet Shoemaker-Levy 9 on Jupiter in July, 1994 was the largest, most energetic impact event on a planet ever witnessed. Because it broke up during a close encounter with Jupiter in 1992, it was bright enough to be discovered more than a year prior to impact, allowing the scientific community an unprecedented opportunity to assess the effects such an event would have. Many excellent observations were made from Earth-based telescopes, the Hubble Space Telescope (HST) and the Galileo spacecraft en route to Jupiter. In this paper, these observations are used in conjunction with computational simulations performed with the CTH shock-physics hydrocode to determine the sizes of the fifteen fragments that made discernible impact features on the planet. To do this, CTH was equipped with a radiative ablation model and a post-processing radiative ray-trace capability that enabled light-flux predictions (often called the impact flash) for the viewing geometries of Galileo and ground-based observers. The five events recorded by Galileo were calibrated to give fragment size estimates. Compared against ground-based and HST observations, these estimates were extended using a least-squares analysis to assess the impacts of the remaining ten fragments. Some of the largest impacts (L, G and K) were greater that 1 km in diameter but the density of the fragments was low, about 0.25 g/cm^3. The volume of the combined fifteen fragments would make a sphere 1.8 km in diameter. Assuming a pre-breakup density of 0.5 g/cm^3, the parent body of Shoemaker-Levy 9 had a probable diameter of 1.4 km. The total kinetic energy of all the impacts was equivalent to the explosive yield of 300 Gigatons of TNT.

Introduction

In early July, 1992, periodic comet Shoemaker-Levy 9 broke up during a close encounter with Jupiter. For a brief two year period, about 20 large fragments and associated debris followed one last orbit about Jupiter before striking the planet at an estimated velocity of 60 km/s. The largest fragments entered the Jovian atmosphere during the week of July 16-22, 1994. Although the impact sites were located just beyond the limb of Jupiter and were not directly visible from Earth, the Galileo spacecraft was positioned for direct viewing of the impact sites. While impact phenomena were not spatially resolved by the spacecraft, its timing, spectral and luminosity data are invaluable for comparison with analytical and numerical models. Fireballs and plumes generated by the impacts were visible in line-of-sight from Earth within a minute (Fig. 1) and the impact locations themselves rotated into view within 7-20 minutes (Hammel *et al.*, 1995). The wealth of data provided by this fortuitous event gives us an opportunity to assess models of meteoroid entry into planetary atmospheres and, in the context of this paper, to estimate the size of the Shoemaker-Levy 9 parent body based on observations of the radiated light flux observed by the Galileo spacecraft and by Earth-based telescopes. The eventual goal of our modeling effort is to provide a mechanism to assess the specific hazard associated with a large atmospheric entry event on Earth (Boslough and Crawford, this volume).

Entry into the Atmosphere

Understanding the mechanisms of kinetic energy loss during meteoroid traversal of planetary atmospheres is crucial for understanding the development of fireballs and plumes that were observed during the impact of Comet Shoemaker-Levy 9 on Jupiter (Crawford, 1996) and entry events in Earth's atmosphere (Boslough and Crawford, this volume). Analytical models of the deceleration, ablation, deformation and breakup of meteoroids during passage through planetary

atmospheres have been proposed and refined by many researchers (Ivanov & Yu, 1988; Zahnle, 1992; Hills & Goda, 1993; Ceplecha *et al.*, 1993; Sekanina, 1993). Here, a modified ablation model is proposed to describe comet entry at high altitudes. The model properly satisfies conservation of energy during the ablative process and can be reconciled with observations of terrestrial meteors. At lower altitudes, the dynamic pressure experienced by the fragment exceeds the compressive yield strength and the fragment deforms hydrodynamically according to the well known 'pancake model' of Zahnle (1992). The current comprehensive model, calibrated against numerical simulations, describes meteoroid entry over a wide range of velocities and spatial scales.

A comet fragment entering Jupiter's atmosphere at hypervelocity produces a parabolic bow shock (Fig. 2). Some of the irreversible heating at the shock is radiatively coupled to the fragment surface causing vaporization of the cometary materials. Because the energy required to remove a unit mass from the surface of the body (by stripping and deceleration) is much greater than the heat of vaporization, a vapor layer forms and thickens. The coupled differential equations that describe the evolution of the vapor layer and the deceleration and hydrodynamic deformation of the fragment are written as:

$$m\frac{dv}{dz} = \frac{C_d}{2}\pi(r+x)^2\rho v\sec\theta \tag{1}$$

$$\frac{dm}{dz} = C_m\pi(r+x)^2\rho\sec\theta \tag{2}$$

$$\frac{dx}{dz} = \frac{C_h R}{8Q_0 A}T_v\left(\frac{r}{r+x}\right)^2\sec\theta - \frac{1}{4}\frac{C_m R T_v}{Av^2}\sec\theta \tag{3}$$

$$r\frac{d^2r}{dz^2} + \frac{r}{v}\frac{dv}{dz}\frac{dr}{dz} = \frac{C_d\rho}{2\rho_f}(\sec\theta)^2 \tag{4}$$

where m, v, r, ρ_f, θ, z, Q_0, and A are the mass, velocity, radius, density, entry angle, altitude, heat of vaporization and average molecular weight of the entering fragment; ρ is atmospheric density;

C_d~1, C_m~0.5 and C_h~10^{-4}-10^{-2} are drag, mass-loss and heat-transfer coefficients; x and T_v are the thickness and temperature of the vapor layer and R is the gas constant. Equation (1) is the well known drag equation. Equation (2) describes mass stripped from the vapor layer by friction with the Jovian atmosphere. The stripped mass is equal to a fraction (C_m~0.5) of the encountered atmospheric mass at any time. The first term to the right of Equation (3) describes the growth of the vapor layer due to radiative ablation. It is obtained by equating the vapor pressure with the kinematic 'ram' pressure (ρv^2). The second term describes deflation of the vapor layer due to the mass loss of Equation (2). Finally, Equation (4) describes the mechanical flattening of the fragment due to hydrodynamic forces near the termination of its flight (after Zahnle, 1992).

Because the radiant energy that drives vaporization at the surface of the meteoroid must propagate through the vapor layer from the bow shock, growth of the vapor layer will slow as the vapor thickens. This leads to a scaling law for the heat transfer coefficient (C_h) which, as we will see, is inversely proportional to fragment size. Growth of the vapor layer is slowed by mass loss from small-wavelength Kelvin-Helmholtz instabilities that develop along the interface with the atmosphere (Roulston and Ahrens, 1996). The vapor reaches an equilibrium thickness (x_m) found by equating the two right-hand terms of Equation (3):

$$x_m = \left(v \sqrt{\frac{C_h}{2 C_m Q_0}} - 1 \right) r . \qquad (5)$$

For small meteoroids, x_m may be several times the radius of the entering body.

Equations (1) - (4) are numerically integrated to determine the deceleration, ablation, vaporization and hydrodynamic deformation experienced by an entering body. The heat transfer coefficient (C_h) is calibrated against numerical multi-material shock physics simulations (a specially-modified version of the CTH shock-physics code; McGlaun, *et al.*, 1990) incorporating radiative ablation. The reduction in vapor volume with increasing fragment size apparent in these simula-

tions (Figs. 3 and 4), is caused by a reduction in heat transfer efficiency as the vapor layer obstructs radiation from the shock front. The heat transfer coefficient is determined by fitting Equations (1)-(4) to the energy deposition per unit altitude derived from the CTH simulations (Fig. 5) and is found to be $C_h = 1/d$ (where d is fragment diameter in meters). This scaling law is consistent with fitted values of C_h for terrestrial meteors ($C_h = 0.03$-0.3; $d < 10$ m). In the following sections, we use the semi-analytical model described by Equations (1)-(4) to provide driving conditions for further CTH simulations of Shoemaker-Levy 9 fireballs and plumes.

Plume Morphology: Comparison with Observations

Simulations performed prior to the impact of Comet Shoemaker-Levy 9 using the CTH shock-physics code compare well qualitatively with many of the observations (Crawford, *et al.*, 1994, 1995). Nevertheless, good quantitative models of the event are required in order to extract useful information from observations of the events. Fortunately, models are strongly constrained by the excellent data collected, especially: (1) the direct light-flux observations made by the Galileo spacecraft (Chapman, 1996); (2) the seemingly contradictory observations that plumes observed by the Hubble Space Telescope (HST) all had approximately the same maximum altitude yet the pattern of dark ejecta they left in the Jovian stratosphere varied considerably in albedo and lateral extent (Hammel *et al.*; 1995, Hammel, 1996); and (3) the Earth-based telescope observations of the infrared impact light flashes (Nicholson, 1996). By using the semi-analytical meteoroid entry model as initial conditions for plume evolution models we can investigate the Shoemaker-Levy 9 events in the context of matching light-flux and plume-height observations.

The technique we use to drive CTH simulations with the results of the semi-analytical entry model is illustrated in Figure 6. With the simulations driven in this way, we can efficiently run computational fireball simulations to investigate differences due to the size of the impactor with-

out having to run time-consuming fully resolved entry calculations for each case. We have performed simulations for ten test cases with comet fragments ranging in size from 250 to 1250 m in diameter. In all cases, we assumed the comets were of density 0.95 g/cm^3 or 0.25 g/cm^3 with an equation-of-state (including melting, vaporization, dissociation and ionization) appropriate for water ice. A two dimensional representation, symmetric to the 45° entry angle, was used to simulate the first few minutes of fireball evolution in CTH. Tracer particles were added to the simulations to represent the Jovian cloud layers.

Figures 7, 8 and 9 show results from two of the numerical fireball simulations that we have performed. The location of cometary debris within the developing plume is shown in the temperature plots of Figure 7. In all cases, the debris front is traveling upwards (along the 45° trajectory) too quickly to make a plume only 3300 km high, the maximum altitude observed by HST. The plots in Figure 8 show that material originating from the Jovian cloud layers (also shown in Figure 8) is climbing at nearly the correct velocity to produce 3300 km plumes and their altitude seems to be relatively independent of impactor size. However, opaque materials from the cloud tops (NH_3, for example) is less than 1%, by mass, of the atmospheric gases within the clouds. By contrast, opaque cometary material makes up about 30% of the mass within the debris front, hence cloud materials are unlikely to compete with cometary debris as a significant source of opacity for the plumes. The maximum altitude of a specific isodensity contour within the cometary debris ejected as part of the plume is an invariant function of fragment size and mass. Hence, it is probable that the tops of the HST plumes, depending on the opacity of condensed cometary materials, are represented by a specific isodensity contour.

To get a better idea of the morphology of the plumes seen by HST, we can estimate the optical properties of cometary material and Jovian atmospheric materials and plot the optical mean-

free-path at wavelengths typical of the HST imagery. Figure 9 shows the inverse mean-free-path (at 890 nm wavelength) for plumes produced by 750-m and 1250-m fragments approximately two minutes after impact. The plots have a mean-free-path upper bound of 10 m (bright white) and are representative of what the plumes would look like if fully illuminated by sunlight. (The actual events occurred in darkness on Jupiter's far side but tops of the plumes climbed high enough to shine in reflected sunlight and be seen from Earth.)

The opacity model for cometary debris is based on the work of Nemtchinov et al. (1996), modified to include opacity of 1 μm condensate particles (using simple geometric cross-section) at temperatures below 3200 K. While condensation of cometary debris is important for matching the temperature data of the late-time plumes (Carlson, et al., 1996), it has only marginal effect on entry light curves, as will be shown later. The opacity model for Jovian air is from Chevalier and Sarazin (1994). Figure 9 demonstrates that the optical properties of the Shoemaker-Levy 9 impact plumes coupled with a dynamic impact process that produces invariant isodensity contours, generate constant maximum plume height even though cometary debris can be found on trajectories well above the apparent plume top.

The model plumes have a characteristic mushroom shape. If ballistically extrapolated forward in time until re-impact with the planet, these plumes are crescent-shaped and have a radial extent (dependent on impactor size and composition) that agree with the observed ejecta patterns. With confidence that our model can describe the morphology of the Shoemaker-Levy 9 plume-forming impacts, we can provide quantitative estimates of fragment sizes by comparing simulated radiative output with observations from the Galileo spacecraft and Earth-based telescopes.

Radiative Output: Comparison with Observations

Figure 10 shows the scheme used to estimate light flux from a typical plume-forming simula-

tion. To estimate light output at a particular wavelength, we integrate the Planck equation radially inwards until the optical limit is reached (at approximately one mean-free-path). During this process, absorption of light by intervening layers of material is taken into account. A realistic outcome to this process requires accurate opacity tables which, generally, depend on density and temperature for the materials involved. For cometary vapor, the opacity tables of Nemtchinov *et al.* (1996) are used. The opacity of clean Jovian air is modeled with mean opacity data from Chevalier and Sarazin (1994).

Figure 11 shows light curves, scaled for distance to the Galileo spacecraft, for three of the five plume-forming events that we have simulated. Shown on the same figure are light curves for several events observed by Galileo's PPR sensor at a wavelength of 945 nm. By comparing with our simulations, we estimate that fragments L, G, H and Q1 were 1250, 1000, 650 and 250 meters in diameter, respectively.

Surprisingly, fragment density plays a significant role in the character of the light curves. Near infrared light emitted from fireballs formed from relatively high density impactors is enhanced at late times (Fig. 11). Since the Galileo light curves did not exhibit significant enhancement at late times, this suggests that the fragments had low average density (0.25 g/cm^3) at time of impact.

The light flux shown in Figure 11 exhibits $d^{1/2}$ scaling, where d is fragment diameter. This occurs because light is emitted from a column that has length solely dependent on the scale height (H) of the atmosphere and a radius proportional to the cometary debris radius ($r_d = r+x_m$). From Equation (5):

$$r_d = r + x_m = vr\sqrt{\frac{C_h}{2C_m Q_0}} = v\sqrt{\frac{C_0 r}{2C_m Q_0}} \qquad (6)$$

where $C_h = C_0/r$ (C_0 is independent of radius) and the area visible to Galileo ($\propto r_d H$) is propor-

tional to $r^{1/2}$.

Many researchers have concluded that dust, mostly material from the impactors, was widely disseminated by the Shoemaker-Levy 9 impact sites (West, 1996) and may be important during the evolution of the fireballs (Carlson *et al.*, 1996). Figure (12) shows light curve simulations assuming a simple model that neglects radiative energy loss and assumes that a single temperature adequately describes the materials that are emitting light. After the initial meteor entry rise and a brief plateau, the light flux begins to rise until it reaches unrealistic levels. In comparison, a more realistic model is produced assuming a two temperature model where cometary vapor below 3200 K is allowed to condense. Because the condensates are probably very opaque, consisting of various metallic oxides, metals and silicates, they are efficient emitters of radiation and cool rapidly. The loss of energy (now approximately accounted for) prevents the dramatic late-time rise (Fig. 12). The differences between the two models yields a small uncertainty (10-20%) of the fragment size estimates. Other sources of uncertainty include noise in the data and the enhanced signal due to light reflected off Jupiter's clouds (to add an additional uncertainty of 10-20%)

Table I shows our estimated sizes for the Shoemaker-Levy 9 fragments that produced discernible features on the planet. The fragment diameter is estimated from a least squares analysis incorporating Galileo light-flux observations (calibrated against CTH light-output calculations) and assuming r^3 dependence (mass scaling) of the peak flux for a given wavelength observed from Earth-based telescopes (Lagage, *et al.*, 1995; Takeuchi, *et al.*, 1995; McGregor, *et al.*, 1996; Nicholson, 1996). For fragments that produced the smallest impact features on the planet, we assumed a constant diameter within the site classification derived from HST imagery (Hammel, 1996).

For most cases where sufficient overlap between the Galileo and Earth-based observations

exists, the r^3 scaling law holds fairly well. Normal variations due to density heterogeneity among the fragments is expected. There are a couple of notable exceptions, however. Fragments Q1 and W were relatively small by Galileo light flux estimates but of moderate size based on Earth-based observations. This could be explained if they were denser than the other fragments (e.g. fully dense silicate vs. fluffy, muddy water ice).

Other researchers have used the Galileo light flux observations to make estimates of fragment size. Nemtchinov *et al.* (1997) estimated diameters of 800, 400 and 300 m for fragments K, W and N respectively based on comparisons of the entry flash with radiative hydrodynamic simulations. These are comparable to the estimates of this study, especially when one considers that the K event light curve (measured with Galileo's solid-state imaging camera), has a distinctly different character than light curves of other comparable events (e.g. L and H) measured with a different instrument. Our estimate for fragment K diameter would agree almost exactly with the results of Nemtchinov *et al.* (1997) if *only* the entry light flash was modeled. A comparison with terrestrial observations, however, suggests that the K and G fragments are of comparable size and that the K light curve is curiously truncated (perhaps from high altitude clouds?).

Carlson *et al.* (1996) have estimated the size of the G impactor as 200-400 meters based on a detailed semi-analytical investigation using multi-wavelength time-dependent observations made by Galileo of this event. In their analysis, they assume that the debris front emitted radiant energy as a blackbody and was optically thick along its entire length. This is a good constraint for a lower bound of the size estimate for that reason. More realistic, density- and temperature-dependent opacity models (performed by Nemtchinov *et al.,* 1997 and this study) seem to produce less light for a given impactor diameter, requiring larger impactors.

For Fragment G to be only 200-400 meters would require smaller fragments like H and K to

explode above Jupiter's cloud tops according to most hydrodynamic deformation models. Normally, the rapid rise of the entry flash is truncated by arrival at the cloud tops (which occludes radiation from deeper) and the distinctive plateau of the light curve is produced. Explosions above the clouds would produce distinctly different light curves for these events (there would be no truncation or plateau), yet the fragment H and K light curves exhibited similar behavior as the larger events (Fig. 11).

Conclusion

The fragments of Shoemaker-Levy 9 that hit Jupiter with discernible effect have a total volume that would make a 1.8±0.5 km diameter sphere at an average density of 0.25 g/cm^3. This is consistent with the total volume of dusty debris seen on the planet after the impacts, corresponding approximately to a 1-km diameter sphere (West, 1996), assuming a typical debris particle density of (1-2 g/cm^3). With a pre-breakup density of 0.5 g/cm^3 (Scotti and Melosh, 1993; Asphaug and Benz, 1994), the parent body had a diameter of 1.4±0.4 km. With these parameters, the Shoemaker-Levy 9 family pummeled Jupiter with the energy equivalent of 300 Gigatons of TNT.

Acknowledgments

Sandia is a multiprogram laboratory operated by Sandia Corporation, a Lockheed Martin Company, for the United States Department of Energy under Contract DE-AC04-94AL85000. Additional funding came from NASA.

References

Asphaug, E. and Benz, W. (1994), Density of Comet Shoemaker-Levy 9 deduced by modelling breakup of the parent 'rubble pile', *Nature, 370*, 120-124.

Carlson, B. *et al.* (1997), Temperature, Size and Energy of the Shoemaker-Levy 9 G-Impact fireball, *Icarus*, (in press).

Ceplecha, Z. *et al.* (1993), Atmospheric fragmentation of meteoroids, *Astron. and Astrophys., 279*, 615-626.

Chapman, C. R. (1996), Galileo observations of the impacts, in *The Collision of Comet Shoemaker-Levy 9 and Jupiter*, K. S. Noll, H. A. Weaver and P. D. Feldman, eds., Cambridge Univ. Press, 121-132.

Chevalier, R. A. and Sarazin, C. L. (1994), Explosions of Infalling Comets in Jupiter's Atmosphere, *Astrophys. J., 429*, 863-875.

Crawford, D. A. *et al.* (1994), The Impact of Comet Shoemaker-Levy 9 on Jupiter, *Shock Waves, 4*, 47-50.

Crawford, D. A. *et al.* (1995), The Impact of Periodic Comet Shoemaker-Levy 9 on Jupiter, *Int. J. Impact Engin., 17*, 253-262.

Crawford, D. A. (1996), Models of Fragment Penetration and Fireball Evolution, in *The Collision of Comet Shoemaker-Levy 9 and Jupiter*, K. S. Noll, H. A. Weaver and P. D. Feldman, eds., Cambridge Univ. Press, 133-156.

Hammel, H. B. *et al.* (1995), HST Imaging of Atmospheric Phenomena Created by the Impact of Comet Shoemaker-Levy 9, *Science, 267*, 1288-1296.

Hammel, H. B. (1996), HST imaging of Jupiter shortly after each impact: Plumes and fresh sites, in *The Collision of Comet Shoemaker-Levy 9 and Jupiter*, K. S. Noll, H. A. Weaver and P. D.

Feldman, eds., Cambridge Univ. Press, 111-120.

Hills, J. G. and M. P. Goda (1993), The Fragmentation of Small Asteroids in the Atmosphere, *Astro. J., 105,* 1114-1144.

Ivanov, B. A. and O. Yu (1988), Simple Hydrodynamic Model of Atmospheric Breakup of Hypervelocity Projectiles, *Lun. Planet. Sci., 19*, 535-536.

Lagage, P. O. *et al.*, (1995), SL-9 fragments A, E, H, L, Q1 collision on to Jupiter: Mid-infrared light curves, *Geophys. Res. Lett.*, 22, 1773.

McGlaun, J. M., Thompson, S. L. and Elrick, M. G. (1990), CTH - A Three-Dimensional Shock-Wave Physics Code, *Int. J. Impact Engin., 10*, 351.

McGregor, P. *et al.* (1996), CASPIR observations of the collision of Comet Shoemaker-Levy 9 with Jupiter, *Icarus*, *121*, 361-388.

Nemtchinov, I. V. *et al.* (1996), Spectral Opacities and Ablation Rates for Recognized Meteoroid Materials, Interim Report 001 on task 1.0 under the Sandia National Laboratories Contract AS-6889, Institute for Dynamics of Geospheres, Russian Academy of Sciences, Moscow, 136 pp.

Nemtchinov, I. V. *et al.* (1997), Assessment of Comet Shoemaker-Levy 9 Fragment Sizes Using Light Curves Measured by Galileo Spacecraft Instruments, *Planet. Space Sci., 45*, 311-326.

Nicholson, P. D. (1996), Earth-based observations of impact phenomena, in *The Collision of Comet Shoemaker-Levy 9 and Jupiter*, K. S. Noll, H. A. Weaver and P. D. Feldman, eds., Cambridge Univ. Press, 81-109.

Roulston, M. S. and T. J. Ahrens (1997), Impact Mechanics and Frequency of SL9-Type Events on Jupiter, *Icarus*, *126*, 138-147.

Scotti, J. V. and Melosh, H. J. (1993), Tidal Breakup and Dispersion of P/Shoemaker-Levy 9:

Estimate of Progenitor Size, *Nature, 365*, 7333.

Sekanina, Z. (1993), Disintegration phenomena expected during the forthcoming collision of periodic comet Shoemaker-Levy 9 with Jupiter, *Science, 262*, 382.

Takeuchi, S. *et al.*, (1995), Near-IR imaging observations of the cometary impact into Jupiter: Time variation of radiation from impacts of fragments C, D and K, *Geophys. Res. Lett., 22*, 1581.

West, R. A. (1996), Particulate matter in Jupiter's atmosphere from the impacts of Comet P/Shoemaker-Levy 9, in *The Collision of Comet Shoemaker-Levy 9 and Jupiter*, K. S. Noll, H. A. Weaver and P. D. Feldman, eds., Cambridge Univ. Press, 269-292.

Zahnle, K. (1992), Airburst Origin of Dark Shadows on Venus, *J. Geophys. Res., 97*, 10243-10255.

Zahnle, K. and M. M. Mac Low (1994), The Collision of Jupiter and Comet Shoemaker-Levy 9, *Icarus, 108*, 1-17.

Table 1: Shoemaker-Levy 9 Fragment and Parent Body Size Estimates

Fragment*	HST Class†	2.3 μm Peak (Jy)‡	12 μm Peak (Jy)‡	Diameter (m)♦
A	2a	20	1,200	450
B	3			(50)
C	2a	25		380
D	3	4		200
E	2a	100	1,550	610
G	1	460		1,000•
H	2a	100	2,400	660•
K	1	460		1,000•
L	1	1,000	12,700	1,270•
N	3	0.04		45•
Q2	3			(50)
Q1	2b	90	1,700	600•
R	2b	70	990	530
S	2c	120		640
W	2c	60		490•
Parent	-	-	-	1,400¶

*Fragments F, P2, T, U and V produced no discernible impact features. Fragments J, M and P1 faded from view before impact (Hammel, 1996). The letters I and O were not used.

†from Hammel (1996). Based on first view of the impact site with the Hubble Space Telescope. Class 1 = large dark feature (>10,000 km radius), Class 2 = medium dark feature (4000-8000 km radius), Class 3 = small dark feature (<3000 km radius).

‡Observed light flux of the main infrared event seen from Earth at 2.3 and 12 μm (Lagage, *et al.*, 1995; Takeuchi, *et al.*, 1995; McGregor, *et al.*, 1996; Nicholson, 1996).

♦Diameter is estimated from a least squares analysis incorporating Galileo light-flux observations (marked with • symbol and calibrated against CTH light-output calculations) and assuming r^3 dependence of the peak flux (for a given wavelength) observed from Earth-based telescopes (Nicholson, 1996). Values in parentheses are estimates assuming diameter equivalence within HST class 3. Uncertainty (1 σ) of individual fragment diameter is 15% for fragments A, E, H, L, Q1 and R and 30% for fragments B, C, D, G, K, N, Q2, S and W. Best fitting fragment density is about 0.25 g/cm^3.

¶Assuming a density of 0.5 g/cm^3 before breakup in 1992. The total volume of the fragments would make a sphere 1760 m in diameter (at 0.25 g/cm^3). Uncertainty of these estimates is dominated by uncertainties of the largest fragments (L, K and G), about 25%.

Figure Captions

Figure 1. Simulated fireball from the impact of a 3-km diameter fragment into Jupiter at 60 km/s shown in cross-section, 67 seconds after impact, with the state of New Mexico (about 500 km tall) superimposed for scale. Temperature is represented by color, with highest temperatures at this time step of about 2200 K.

Figure 2. Schematic diagram of the analytical entry model that explicitly models the development and behavior of an ablative vapor layer. The increased interaction cross section, $\pi(r+x)^2$, due to the presence of the vapor, accommodates energy conservation during the ablative process while retaining the potentially large energy deposition rates of previous models. The thickness of the vapor layer, which changes dynamically as the impactor penetrates, is a function of impactor composition, the temperature at the bow shock and the opacity of the vapor and atmospheric gases.

Figure 3. Comparison of four shock physics simulations (using the CTH hydrocode) showing the entry of S-L 9 fragments varying from 250 m to 3 km in diameter (d = 250, 500, 1000 and 3000 m). In addition to the normal hydrodynamics that describe the deformation and eventual breakup of the fragments, the simulations include radiative ablation by computing the flux of electromagnetic energy impinging on the fragment surface and vaporizing a corresponding portion of the impactor material. There are three materials present in the calculations: Jovian atmosphere, water ice (an analog for pristine cometary material) and water vapor (formed by radiative ablation). In these 2D cross-sectional plots, color represents temperature.

Figure 4. Comparison of four CTH simulations showing the entry of S-L 9 fragments four seconds after the time shown in Fig. 2. At this altitude, just below Jupiter's cloud-tops, the aerodynamic pressure is causing severe deformation of most fragments. The 250 m fragment has disrupted, the 500 m fragment is in the process of disrupting, the 1 km fragment is severely deformed and the 3 km fragment is slightly deformed. Fragments smaller than about 200 m disrupt completely above the Jovian cloud tops whereas the largest fragments may penetrate another 100-150 km before final disruption.

Figure 5. Energy deposition from 500-m and 1-km ice fragments entering Jupiter's atmosphere. The solid curves are from CTH simulations incorporating radiative ablation. Results of the semi-analytical model (with C_h values indicated) are superimposed (gray curves).

Figure 6. Schematic diagram showing the technique used to initialize CTH fireball simulations with the semi-analytical model. Shocked atmosphere and vapor are added to the simulation with density, temperature and momentum appropriate for the altitude of the entering fragment.

Figure 7. Plots of the ascending fireball from 750 m and 1250 m diameter (d) fragments seen 40 and 100 seconds after impact. A shock wave develops above the clouds and accelerates upwards along the debris column. After 100 seconds, debris from the comet has reached altitudes of 2000 km and is traveling upwards at 18-25 km/s. The plume has a distinctive mushroom shape which, when landed as ejecta on the planet, produces the crescent-shaped feature seen in telescope images. Color represents temperature. The debris front is indicated by the solid white curve.

Figure 8. Plots of the fireball from 750 m and 1250 m fragments seen 140 seconds after impact. Gray-scale represents log(density). The altitude of the 10^{-13} g/cm^3 isodensity contour (shown by the white curve) and the altitude of material from the Jovian cloud layers, represented by tracer particles (white dots) are invariant with respect to fragment size.

Figure 9. Cross-sectional plots showing plumes resulting from impact of 750 m and 1250 m fragments as they would appear in reflected sunlight. Gray scale represents -log(mean-free-path). The altitude of the 10-m mean-free-path contour (white curve) is nearly invariant with respect to fragment size. The albedo of cometary debris is unknown but probably very low so the brightness of these plots is only a relative indicator.

Figure 10. Scheme used to calculate the light flux, $L_\lambda(t)$, from a CTH shock-physics calculation. The Planck equation with appropriate density- and temperature-dependent opacity tables is integrated radially inwards until the optical limit is reached (at r_0). Radiative output from below the cloud layers is excluded.

Figure 11. Comparison of CTH-simulated light curves (for 250, 500, 750, 1000 and 1250 m fragments) against Galileo spacecraft observations (at 945 nm) of the impacts of fragments L, H and Q1 (solid curves) and G (dots). Gray lines and dashed lines are simulations performed assuming fragment density of 0.25 and 0.95 g/cm^3, respectively.

Figure 12. Comparison of CTH-simulated light curves using molecular opacity tables for cometary vapor from Nemtchinov, et al. (1996) (dashed curves) and modified opacity tables that

accommodate condensation (and consequent radiative decoupling) for temperatures less than 3200 K (solid curves). Fragment diameters of 250, 500, 750, 1000 and 1250 meters are shown. Both sets of curves demonstrate that light flux is proportional to $r^{1/2}$. The discrepancy between the two opacity models in the magnitude of the initial rise yields a 20% uncertainty in fragment size.

Color Figure

Figure 1

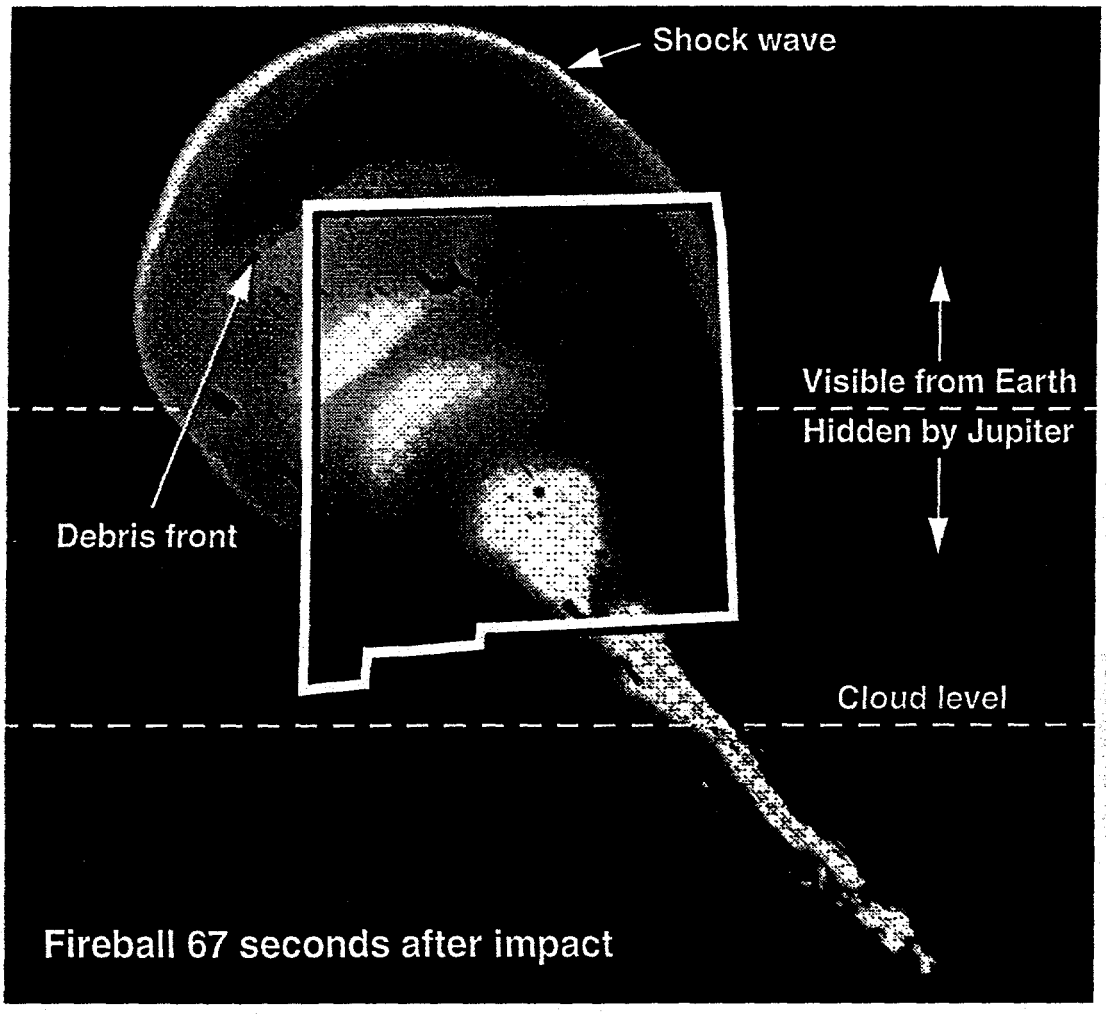

Figure 2

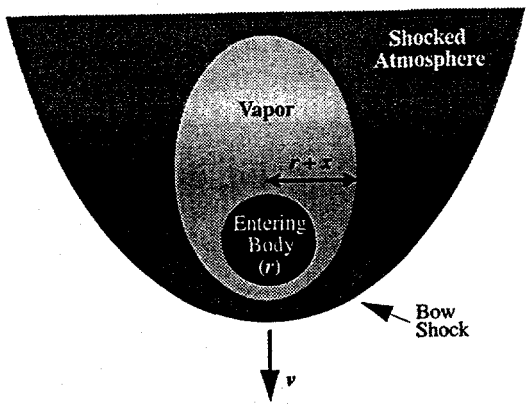

Color Figure

Figure 3

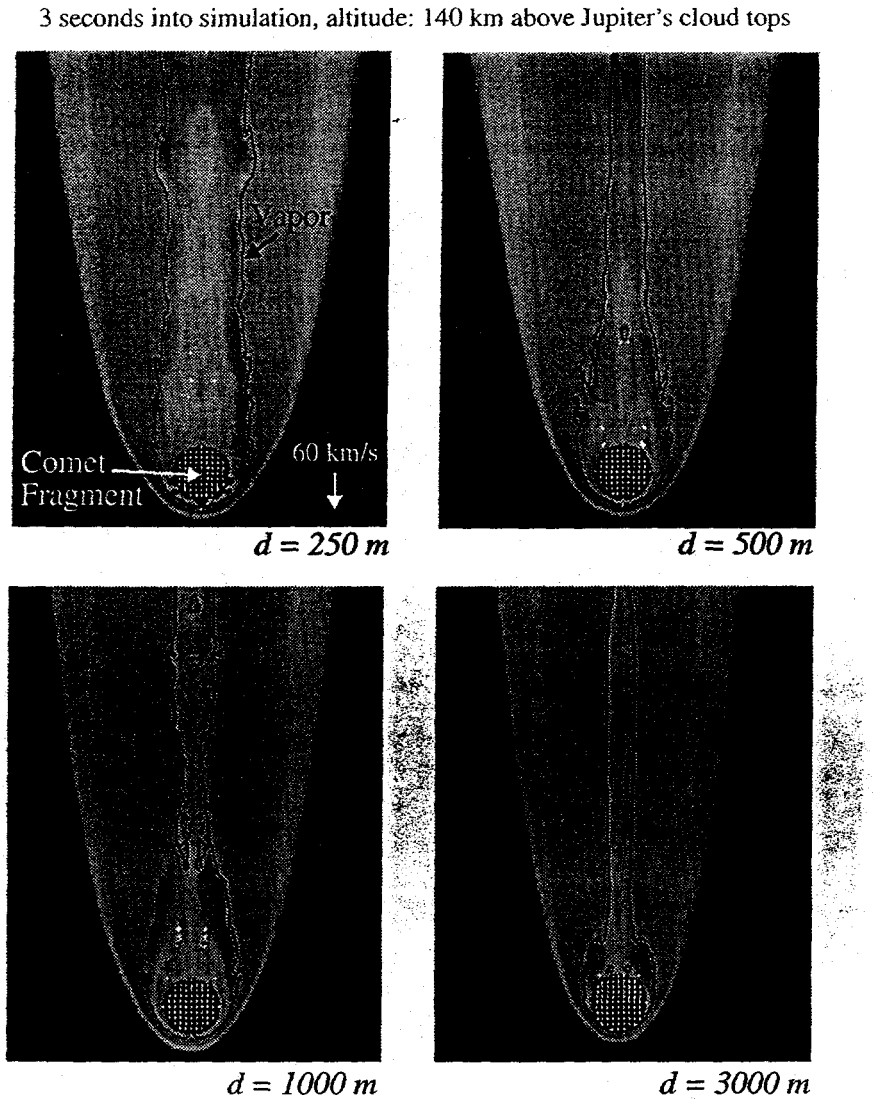

Color Figure

Figure 4

7 seconds into simulation, altitude: 30 km below Jupiter's cloud tops

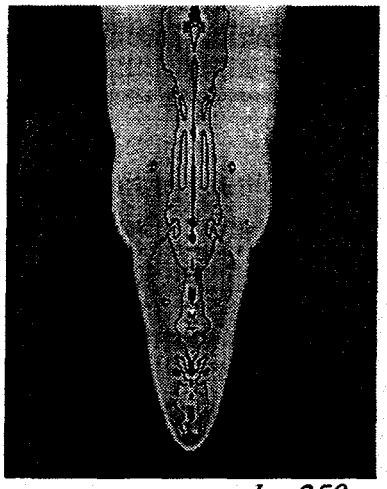

d = 250 m

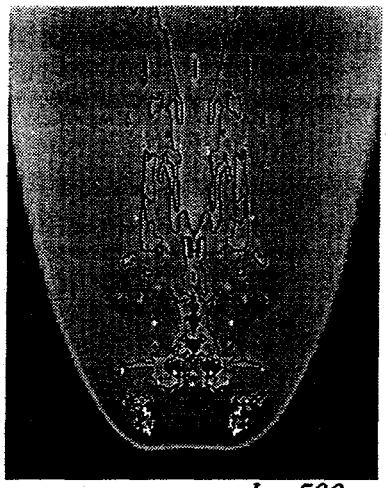

d = 500 m

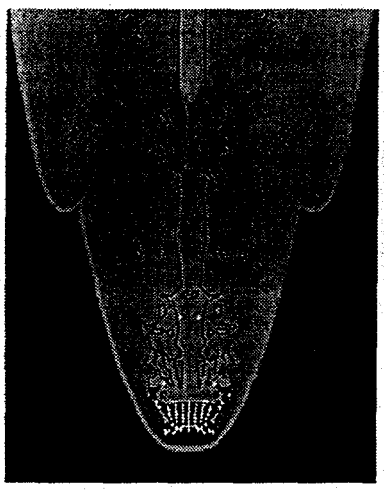

d = 1000 m

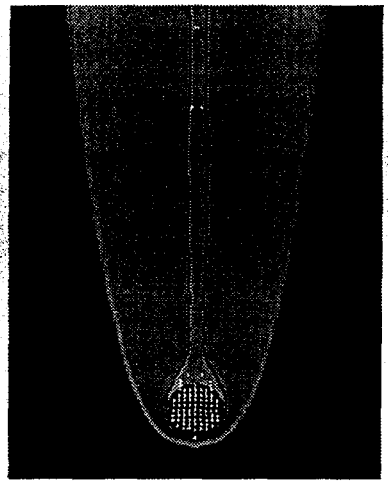

d = 3000 m

Figure 5

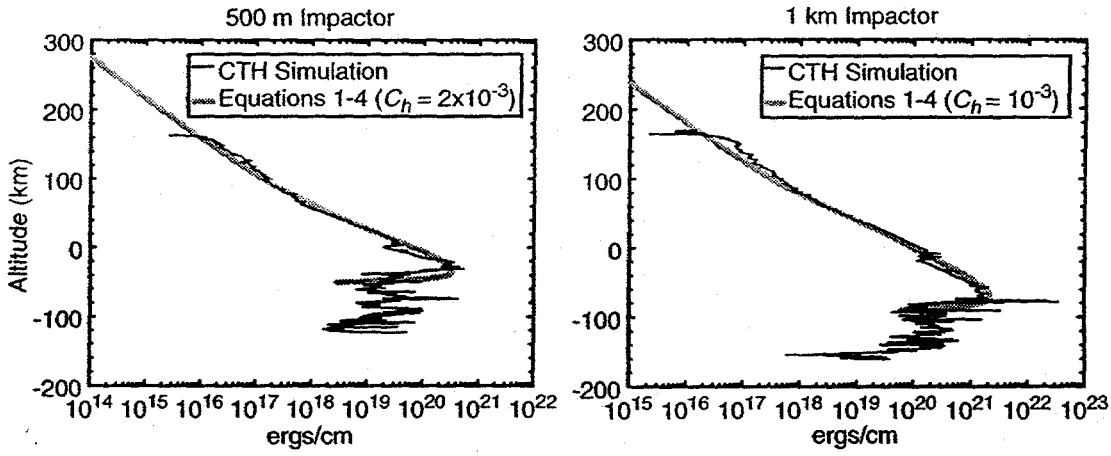
500 m Impactor
1 km Impactor
CTH Simulation
Equations 1-4 ($C_h = 2x10^{-3}$)
Equations 1-4 ($C_h = 10^{-3}$)
Altitude (km)
300
200
100
0
-100
-200
10^{14} 10^{15} 10^{16} 10^{17} 10^{18} 10^{19} 10^{20} 10^{21} 10^{22}
10^{15} 10^{16} 10^{17} 10^{18} 10^{19} 10^{20} 10^{21} 10^{22} 10^{23}
ergs/cm
ergs/cm

Figure 6

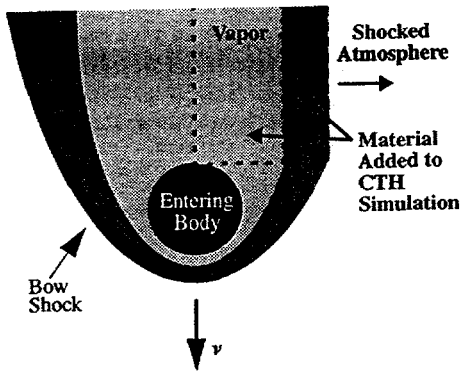
Vapor
Shocked Atmosphere
Material Added to CTH Simulation
Entering Body
Bow Shock
v

Color Figure

Figure 7

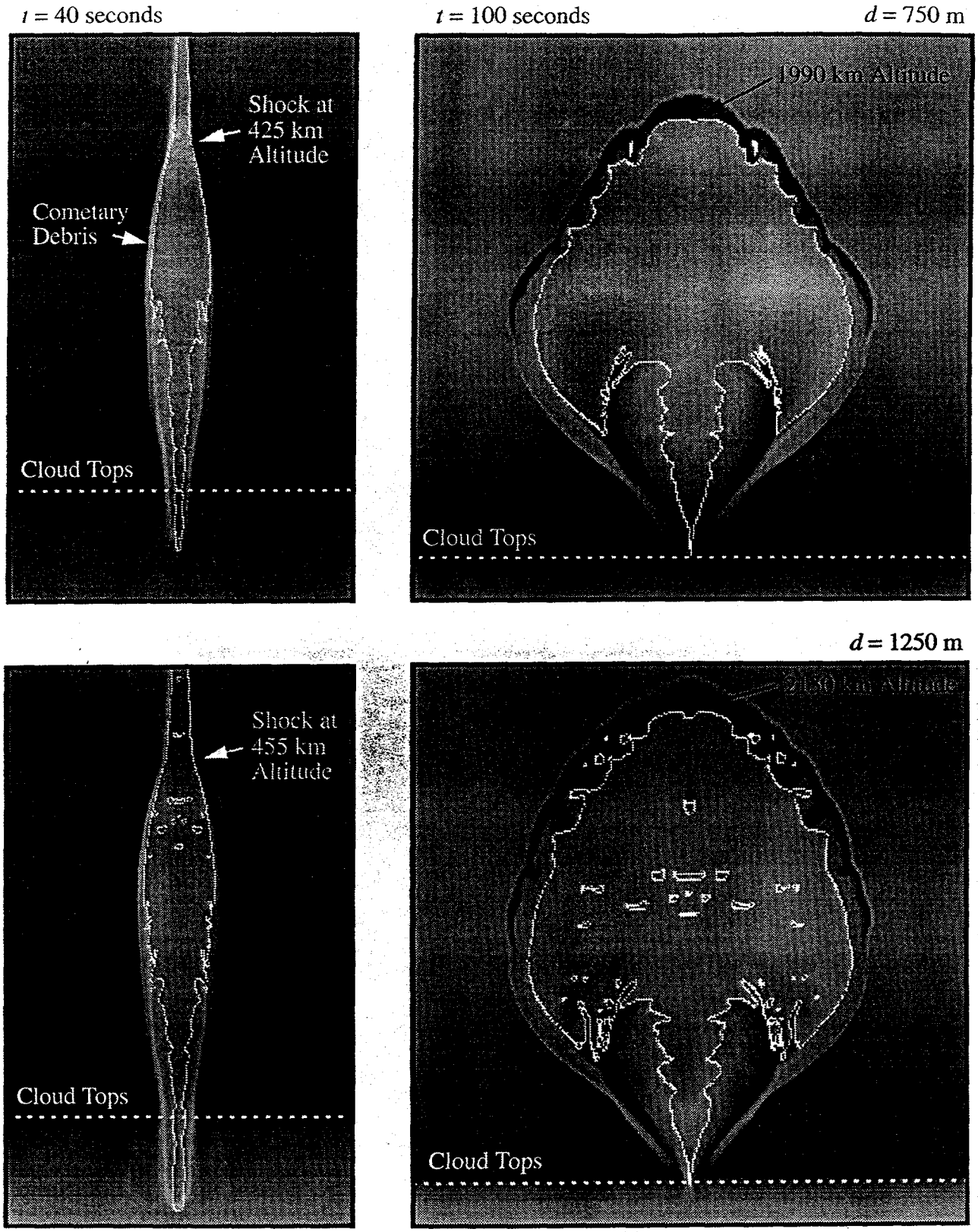

Figure 8

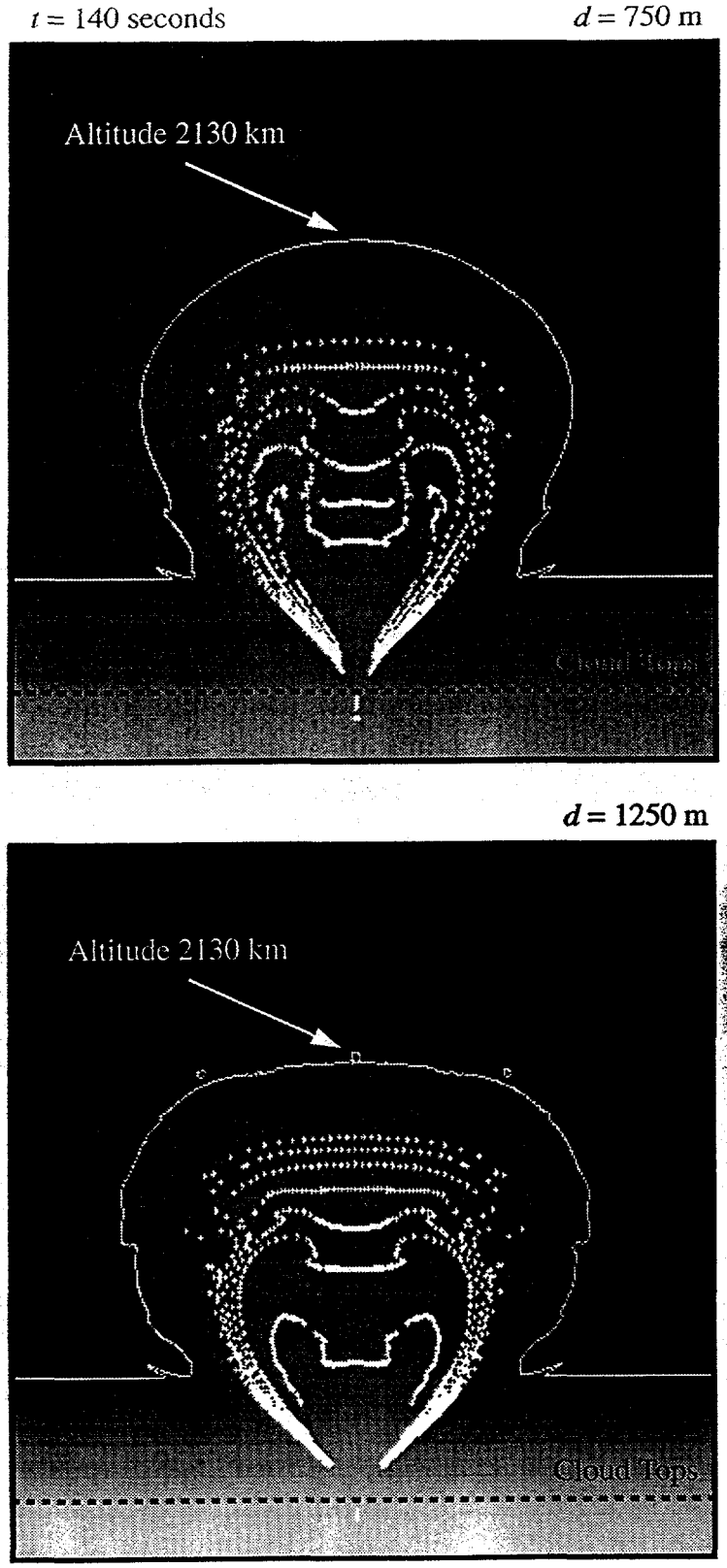
t = 140 seconds
d = 750 m
Altitude 2130 km
Cloud Tops
d = 1250 m
Altitude 2130 km
Cloud Tops

Figure 9

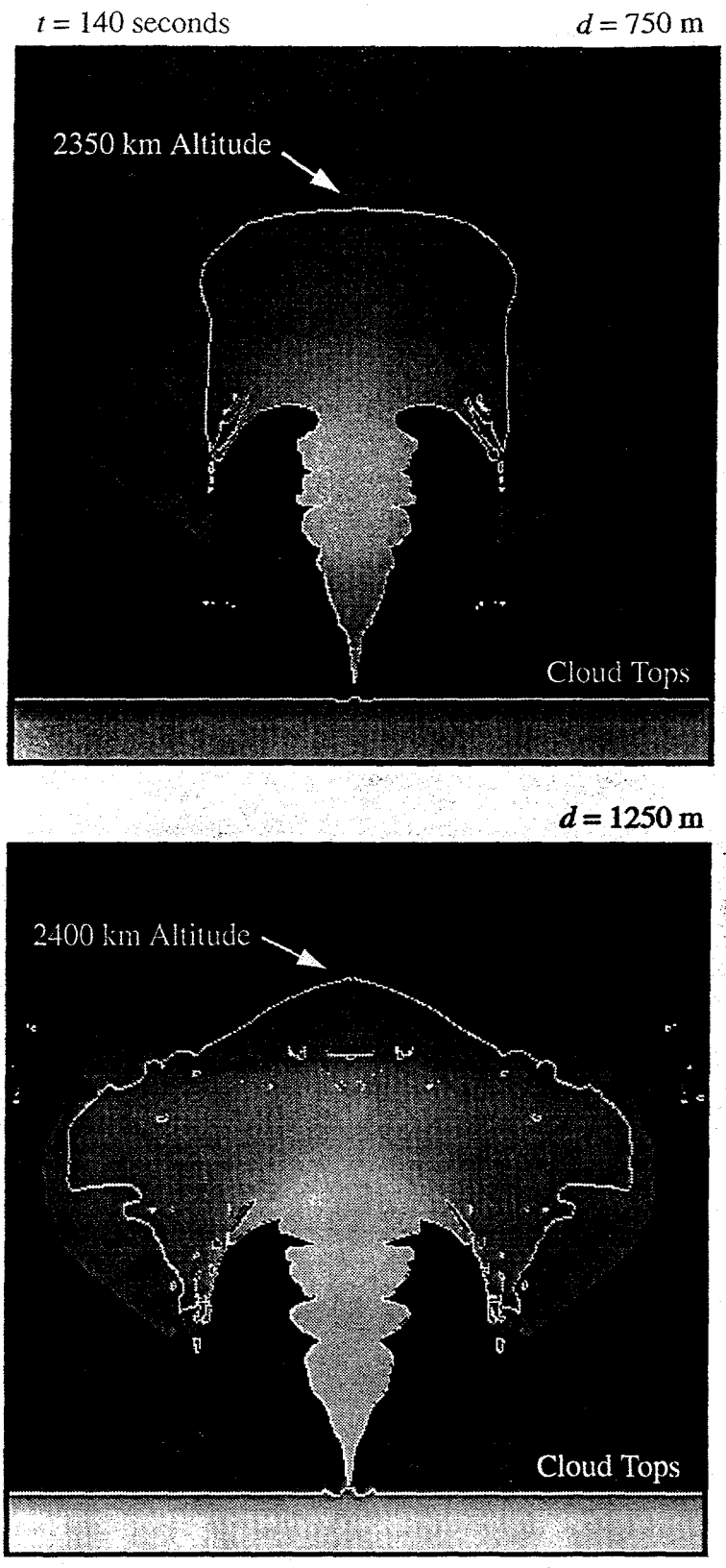
t = 140 seconds
d = 750 m
2350 km Altitude
Cloud Tops
d = 1250 m
2400 km Altitude
Cloud Tops

Color Figure

Figure 10

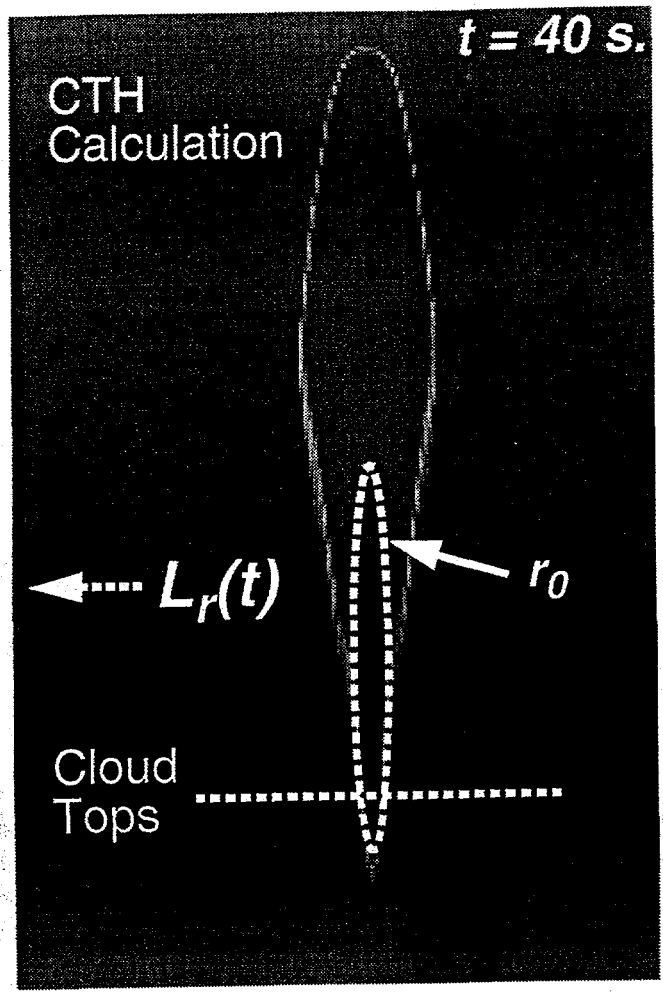

Figure 11

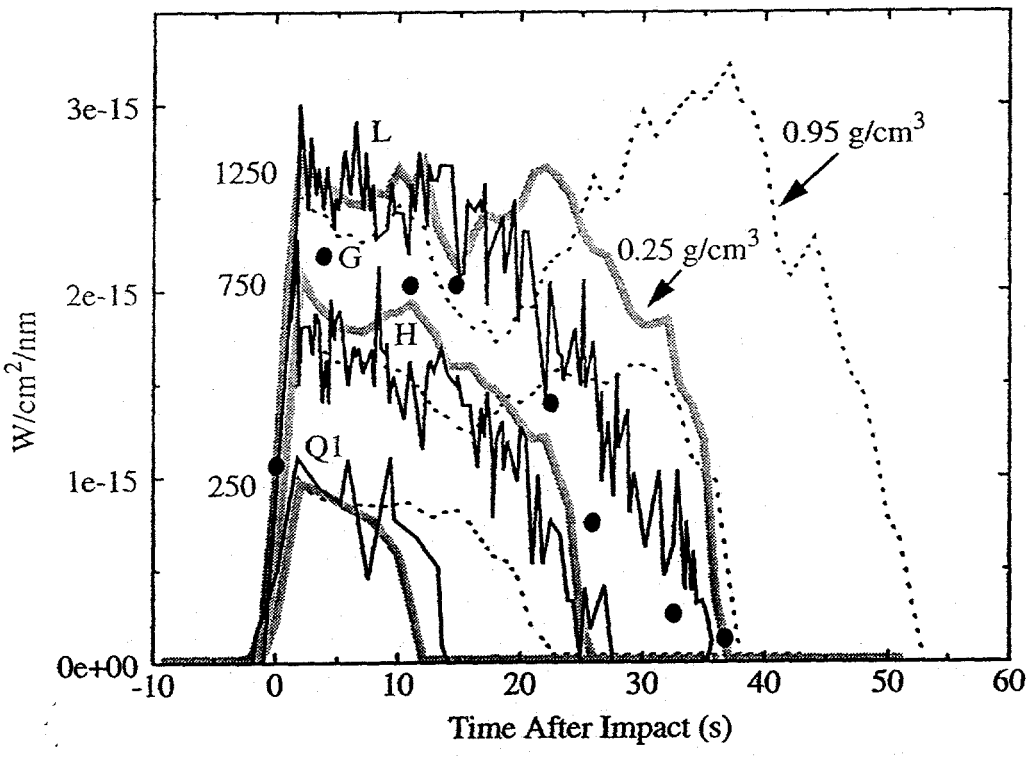
3e-15
2e-15
1e-15
0e+00
W/cm²/nm
1250
750
250
L
G
H
Q1
0.95 g/cm³
0.25 g/cm³
-10
0
10
20
30
40
50
60
Time After Impact (s)

Figure 12

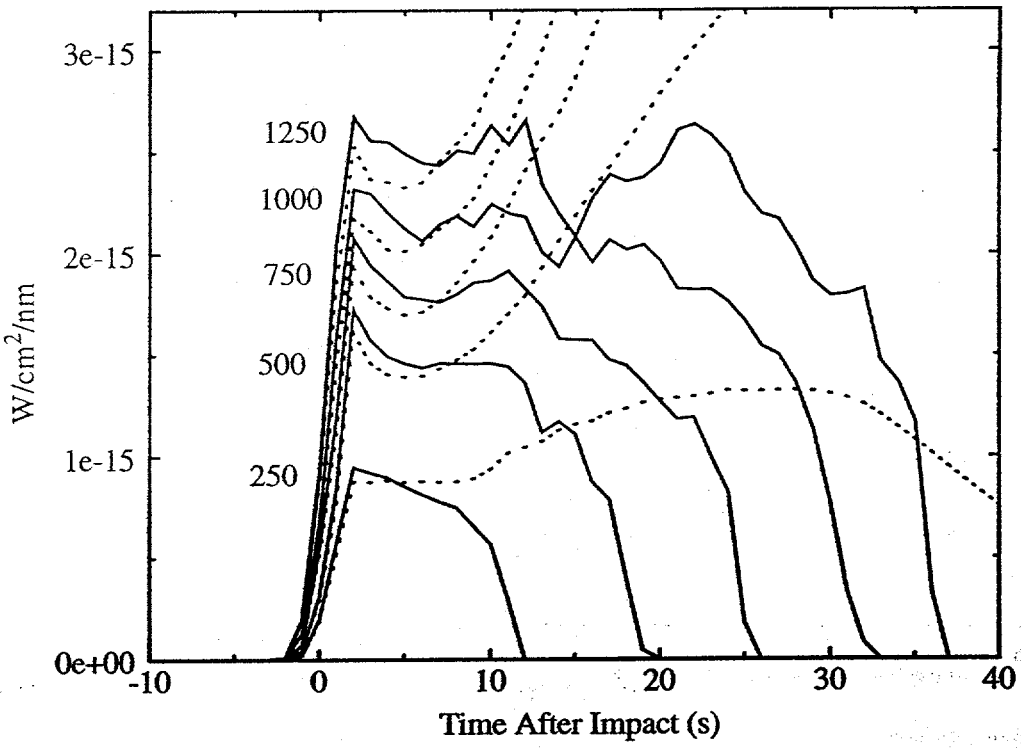
3e-15
2e-15
1e-15
0e+00
W/cm^2/nm
1250
1000
750
500
250
-10
0
10
20
30
40
Time After Impact (s)